Journal of Materials Chemistry C

ROYAL SOCIETY OF CHEMISTRY

PAPER

View Article Online
View Journal | View Issue

Cite this: J. Mater. Chem. C, 2021, 9, 6251

Cyanophenyl spiro[acridine-9,9′-fluorene]s as simple structured hybridized local and charge-transfer-based ultra-deep blue emitters for highly efficient non-doped electroluminescent devices (CIE$y \leq 0.05$)†

Taweesak Sudyoadsuk,[a] Sujinda Petdee,[a] Chokchai Kaiyasuan,[a] Chaiyon Chaiwai,[a] Praweena Wongkaew,[b] Supawadee Namuangruk,[c] Pongsakorn Chasing[a] and Vinich Promarak *[ab]

Received 28th January 2021,
Accepted 5th April 2021

DOI: 10.1039/d1tc00406a

rsc.li/materials-c

The hybridized local and charge-transfer (HLCT) excited state is a successful approach to accomplish both high external and internal quantum efficiency. To obtain deep blue emissive HLCT emitters, two cyanophenyl substituted spiro[acridine-9,9′-fluorene] isomers, namely **SAFmCN** and **SAFpCN**, were designed and synthesized. The photophysical and density functional theory (DFT) results confirmed that both molecules exhibited HLCT features with strong ultra-deep blue emissions in both solution and film states with emission peaks at 410–433 nm. The non-doped OLED devices showed emissions in high-definition television (HDTV) standard blue color (CIE$y \leq 0.05$) with a narrow full width at half maximum (50–56 nm), excellent electroluminescence (EL) performance and a low turn-on voltage of 3.2 V. Particularly, the **SAFpCN**-based device achieved a maximum luminance efficiency (CE) and maximum external quantum efficiency (EQE) of 6.54 cd A^{-1} and 4.63%, respectively.

Introduction

Blue light-emitting diodes (OLEDs) play a crucial role in OLED technologies for applications in both full-color displays and solid-state lighting.[1] Particularly, efficient and stable deep blue OLEDs with Commission Internationale de I'Eclairage (CIE) coordinates of (0.15, 0.06) are vital for high-definition television (HDTV) displays, which is an upcoming display market for OLEDs.[2] Besides, the electroluminescence (EL) performance of deep blue OLEDs has been relatively low compared to those of the green and red ones due to the deep-blue emitter's intrinsic wide-bandgap.[3] So far, there have been several useful strategies for developing deep blue-emitting materials for high-efficiency devices.[1a,4] Blue OLEDs fabricated with typical fluorescence emitters or triplet–triplet fusion (TTF) emitters usually exhibit good deep blue color quality with more excellent operational stability than blue phosphorescent OLEDs.[5] Nonetheless, the efficiency of typical blue fluorescence or TTF emitters is much lower than that of phosphorescence emitters because OLEDs using standard fluorescence or TTF emitters have theoretical limits of maximum internal quantum efficiency (IQE) of 25% and 62.5%, respectively.[5,6] Lately, donor–acceptor (D–A) type thermally activated decayed fluorescence (TADF)[7] and hybridized local and charge-transfer (HLCT)[2a,8] blue-emitting materials have received sizable attention since both emitters can theoretically realize 100% IQE.[4a] Unfortunately, TADF blue OLEDs need an appropriate host with high triplet energy to reduce aggregation quenching and exciton confinement, and suffer from a sharp efficiency roll-off at high current density due to the long-lived first triplet excited state excitons. Simultaneously, deep-blue TADF emitters remain rare due to the bathochromic shift related to intramolecular charge transfer (CT).[9] HLCT-based emitters feature the properties of both a locally-excited (LE) state and a CT state, and the conversion of triplet excitons into singlet excitons *via* reverse intersystem crossing (RISC), giving rise to high photoluminescence (PL) and high exciton utilization efficiencies (η_s).[10] HLCT intrinsically retains short-lived exciton character that can avoid

[a] Department of Materials Science and Engineering, School of Molecular Science and Engineering, Vidyasirimedhi Institute of Science and Technology, Wangchan, Rayong 21210, Thailand. E-mail: vinich.p@vistec.ac.th
[b] Research Network of NANOTEC-VISTEC on Nanotechnology for Energy, Vidyasirimedhi Institute of Science and Technology, Wangchan, Rayong, 21210, Thailand
[c] National Nanotechnology Center (NANOTEC), National Science and Technology Development Agency, Pathum Thani 12120, Thailand

† Electronic supplementary information (ESI) available. See DOI: 10.1039/d1tc00406a

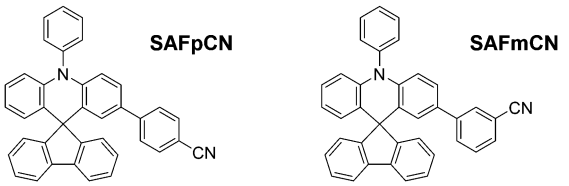

Fig. 1 Molecular structures of two spiro-acridine-based deep blue emitters.

serious efficiency roll-off from long-lived exciton quenching. Based on the HLCT concept, efficient deep blue fluorescence emitters for highly efficient and sable non-doped OLEDs could be achieved since, in HLCT, the LE and CT states are highly hybridized into a new state, relieving largely red-shifted emission from a strong CT state.[2a,11] Recently, some D–A molecules with an HLCT excited state have been reported, with an ultra-high η_s of nearly 100% in OLEDs.[12] However, to date, OLEDs based on HLCT emitters, exhibiting high EL performance and deep-blue emissions with CIE$y \leq 0.05$, have been rarely reported.[2a,11a,13] To accomplish such demand, we herein employ a highly rigid, orthogonal spiro configuration spiro[acridine-9,9′-fluorene] (SAF)[14] as a donor to couple with either *meta*- or *para*-cyanophenyl as an acceptor for forming new D–A type HLCT-based deep blue emitters (**SAFmCN** and **SAFpCN**, Fig. 1). Indeed, **SAFpCN** employed as non-doped emitters notably yielded ultra-deep blue OLEDs with CIE$y \leq 0.05$, narrow emission spectra, and high CE_{max}/EQE_{max} of 6.54 cd A^{-1}/4.63%.

Results and discussion

Two cyanophenyl substituted spiro[acridine-9,9′-fluorene] isomers (**SAFpCN** and **SAFmCN**) were synthesized by a facile three-step procedure as illustrated in Scheme S1 (ESI†). They were isolated as white solids and structurally confirmed by ^{1}H NMR, ^{13}C NMR, and mass spectroscopy (Fig, S8, ESI†) consistent well with their chemical structures.

The optimized structures computed using the B3LYP/6-31G(d,p) function revealed that the fluorene and triphenylamine (TPA) fragments in the SAF unit are nearly perpendicular to each other, showing a sizeable twisting angle of 88° (Fig. 2). This orthogonal geometry is useful for restricting the intermolecular interactions and enhancing the morphological stability.[15] As anticipated, the HOMO distribution is mainly located on the electron-donating TPA unit, while the electron-accepting cyanophenyl part dominates the LUMO, signifying a potential bipolar characteristic (Fig, S1, ESI†). The partial orbital overlap between the HOMO and LUMO would help realize high PL and EL efficiency simultaneously as the emitter applied in OLEDs.[16] The HOMO–LUMO gaps and energy levels of **SAFpCN** were narrower and deeper than those of **SAFmCN**, respectively, due to the *para*-substitution effect of the strong electron-withdrawing cyano group. To describe the excited-state properties of the two molecules, the natural transition orbitals (NTOs) of the $S_0 \rightarrow S_1$ transition calculated using the

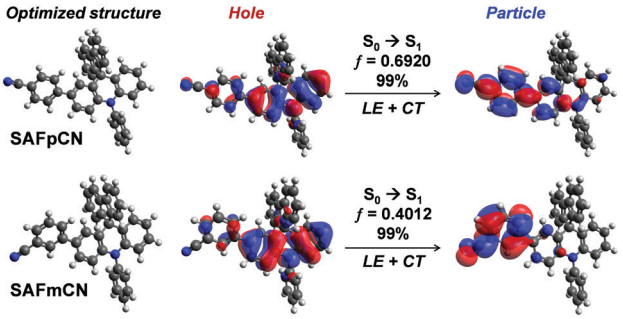

Fig. 2 Natural transition orbitals (NTOs) of the $S_0 \rightarrow S_1$ transition obtained from TDA-B3LYP/6-31G(d,p) calculations (f represents the oscillator strength. The percentage indicates the possibility of the transition).

TD-B3LYP/6-31G(d,p) method clearly showed the HLCT transition characteristics (Fig. 2). The overlap of the hole and particle distribution on the phenyl ring of the TPA unit suggests a LE-like transition, which is essential for high-efficiency fluorescence.

Meanwhile, the separation of holes and particles leads to a CT transition. Thus, the transition of S_0–S_1 should be involved in both LE and CT transition. The overlap density between holes and particles is expanded mainly in **SAFpCN** relative to that of **SAFmCN**, indicating an enhanced LE component in the S_1 state due to the *para*-cyano's significant contribution substitution. The oscillator strength (f) of $S_0 \rightarrow S_1$ transition of **SAFpCN** (0.6920) was also calculated to be higher than that of **SAFmCN** (0.4012), implying that a higher PL could be expected in **SAFpCN** than in **SAFmCN**. As evident from the energy landscape plots (Fig. S2, ESI†), in all cases, the energy gaps between the S_1 and T_2 states ($\sim$0.02 eV) are substantially narrower than that between T_2 and T_1 states (0.77–1.09 eV), indicating that the RISC rate (k_{RISC}) from the T_2 to S_1 state should be higher than the internal conversion rate (k_{ICT}) from the T_2 to T_1 states, giving rise to a possibly hot exciton (short-lived exciton) channel for the RISC of the $T_2 \rightarrow S_1$ process according to the El-Sayed rule.[17]

The excited state features of **SAFpCN** and **SAFmCN** are further evaluated by characterizing their optical properties. As shown in Fig. 3a, the absorption peak at $\sim$312 nm may relate to the π–π* transition of TPA, while the longer wavelength absorption peaks at 340–360 nm may stem from the CT transition from D to A. The two compounds in solution and thin film states displayed strong deep blue emissions peaked at 435 nm and 433 nm for **SAFpCN**, and 418 nm and 410 nm for **SAFmCN**, respectively. The absolute PL quantum yield (Φ_{PL}) of **SAFpCN** in toluene was as high as 84%, reflecting an apparent LE state emission character. In comparison, Φ_{PL} of **SAFmCN** in toluene was only 28%, ascribed to the intrinsic property that the CT state always causes a low PL efficiency.[18] A similar trend was observed in the solid film state, and the Φ_{PL} values for **SAFpCN** and **SAFmCN** were measured to be 45% and 30%, respectively. Both compounds displayed apparent solvatochromic shifts with the increase of solvent polarity from hexane to acetonitrile, indicating that their emissive states are typical CT characters

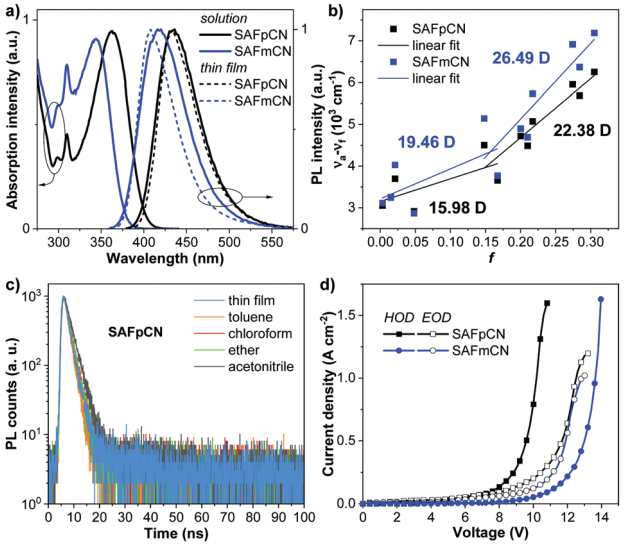

Fig. 3 (a) The absorption and PL spectra in $CHCl_3$ solution (solid line) and neat film (dashed line). (b) Lippert–Mataga plots (*f*, orientation polarizability of solvent media; $\nu_a - \nu_f$, Stokes shift *a*: absorption; *f*: fluorescence). (c) Transient PL decay spectra in solutions and thin films. (d) Current density–voltage (*J*–*V*) plots of the hole (HOD) and electron only devices (EOD).

(Fig. S3 and Table S1, ESI†).[8a] The PL spectra in low-polarity hexane reveal mild vibronic structures, and then the PL spectra gradually broadened and become structureless with the increase in the solvent polarity. The solvatochromic effect was further analyzed by plotting the Stokes shift ($\nu_a - \nu_f$) *vs.* the solvent orientational polarizability (f), according to the Lippert–Mataga equation. As depicted in Fig. 3b, both compounds show two independent slopes of the fitted line suggesting the existence of two different excited-states, whose dipole moments (μ_e), are estimated to be 22.38 D for **SAFpCN** and 26.49 D for **SAFmCN** in high-polarity solvents and 15.98 D for **SAFpCN** and 19.46 D for **SAFmCN** in low-polarity solvents, respectively. The large μ_e values can be considered as a CT-like state, while the small μ_e values should be assigned to the typical excited-state, which is a LE-like state. These results indicate that the emissive states of **SAFpCN** and **SAFmCN** exhibit sufficiently hybridized LE and CT character, consistent with the HLCT state's description.[8a] The presence of the HLCT state could ensure a relatively high PL efficiency and a large fraction of singlet exciton generation in EL.[3] Further time-resolved PL measurements suggested that the PL of both molecules evolves from only one excited state and the HLCT state was supposed to be formed rather than a simple mixture of the LE and CT states, since their PL traces gave single-exponential lifetimes (τ) of 2–5 ns in different solvent polarities and thin films (Fig. 3c).

Thermal property analyses by thermogravimetric analysis (TGA) and differential scanning calorimetry (DSC) confirmed that both **SAFpCN** and **SAFmCN** were thermally stable materials with decomposition temperatures at 5% weight loss (T_{5d}) of as high as 377–387 °C and a glass transition temperatures (T_g) of 94–95 °C (Table 1, Fig. S4, ESI†). Cyclic voltammetry (CV) traces of the two compounds displayed a single reversible oxidation process at a half-wave potential ($E_{1/2}$) of ~1.2 V, assigned to the oxidation of the TPA unit. They exhibited good electrochemical stability and reversibility, as their repeated CV scans showed unchanged CV traces (Fig. S5, ESI†). The HOMO/LUMO energy levels in the thin-film determined by photoelectron yield spectroscopy (AC-2) in air (Fig. S6, ESI†) and the optical band gaps (E_g^{opt}) were estimated to be −5.73/−2.69 eV for **SAFpCN** and −5.64/-2.46 eV for **SAFmCN** (Table 1). Besides, the results of the hole and electron-only devices disclosed that **SAFpCN** possessed better hole mobility and charge balance than **SAFmCN** (Fig. 3d and Table 1). The hole and electron mobilities for **SAFpCN** and **SAFmCN** were calculated by combining the Mott–Gurney equation and Frenkel effect[19] to be 2.90×10^{-6} and 1.86×10^{-6} $cm^2\ V^{-1}\ s^{-1}$, and 1.03×10^{-7} and 1.33×10^{-6} $cm^2\ V^{-1}\ s^{-1}$, respectively.

To evaluate the deep blue EL properties of **SAFpCN** and **SAFmCN** as the emissive layer (EML), non-doped OLEDs were fabricated with the optimized configuration of ITO/MoO_3 (6 nm)/C_{60} (3 nm)/4,4′-cyclohexylidenebis[*N*,*N*-bis(*p*-tolyl)aniline] (TAPC) (20 nm)/**SAFpCN** or **SAFmCN** (40 nm)/1,3,5-tris (3-pyridyl-3-phenyl)benzene (TmPyPB) (55 nm)/LiF (0.5 nm)/Al (150 nm). ITO and LiF/Al were used as the anode and cathode in these devices, respectively, and MoO_3/C_{60} as a hole-injection layer. The high electron mobility of TmPyPB as the electron-transporting and hole-blocking layer and high hole mobility of TAPC as the hole-transporting and exciton blocking layer will possibly regulate the exciton recombination zone width in the EML. In contrast, their suitable energy levels and appropriate band alignments between the layers will facilitate hole/electron accumulation and exciton recombination at the interfaces (Fig. 4a).[20] The non-doped device's characteristics and data

Table 1 Key optical and physical data of **SAFpCN** and **SAFmCN** in solution and solid film states

Compd	λ_{abs} (log(ε))[a] (nm, $M^{-1}\ cm^{-1}$)	λ_{PL} sol[a]/film[b] (nm)[a]	Φ_{PL} sol[a]/film[b] (%)[c]	τ sol[a]/film[b] (ns)[d]	$T_g/T_m/T_{5d}$[e] (°C)	$E_{1/2}$ *vs.* Ag/Ag^+ (V)[f]	E_g^{opt} (eV)[g]	HOMO/LUMO (eV)[h]	Hole/electron mobility[i] ($cm^2\ V^{-1}\ s^{-1}$)
SAFpCN	312(4.27), 360(4.51)	435/433	84/45	2/2	94/273/387	1.12	3.04	−5.73/−2.69	2.90×10^{-6}/1.86×10^{-6}
SAFmCN	312(4.49), 340(4.56)	418/410	28/33	3/3	95/288/377	1.12	3.18	−5.64/−2.46	1.03×10^{-7}/1.33×10^{-6}

[a] Measured in 2×10^{-5} mol L^{-1} $CHCl_3$ solution. [b] Measured in thin-film coated on fused silica substrates. [c] Absolute PL quantum yield measured using an integrating sphere. [d] Transient PL decay of solid films. [e] Determined by DSC and TGA under N_2 flow. [f] Analysed by CV in CH_2Cl_2 containing 0.1 M *n*-Bu_4NPF_6 under argon flow. [g] Estimated from the absorption onset of the solid film: $E_g = 1240/\lambda_{onset}$. [h] HOMO measured by AC-2 of the neat film and LUMO = HOMO + E_g. [i] Determined by using a hole only device (ITO/NPB 10 nm/Compd 80 nm/NPB 10 nm/Al 100 nm) and electron only device (ITO/TmPyPB 10 nm/Compd 80 nm/TmPyPB 10 nm/LiF 0.5 nm/Al 100 nm).

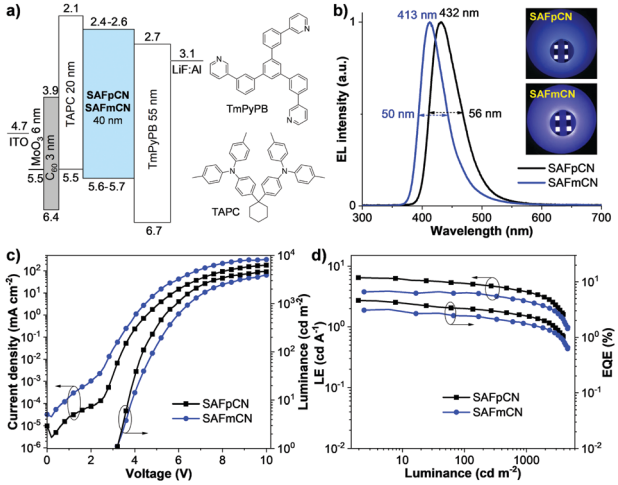

Fig. 4 (a) Schematic energy diagram (relative to the vacuum energy level) and organic materials used in this study, (b) EL spectra (inset: images of OLEDs), (c) current density–voltage–luminance (J–V–L) plots, and (d) EQE–J plots of the fabricated non-doped EL devices.

are shown in Fig. 4 and are listed in Table 2. The **SAFpCN**- and **SAFmCN**-based devices exhibited strong deep blue emissions with λ_{max} at 432 and 413 nm, and CIE of (0.153, 0.054) and (0.160, 0.046), respectively. Although the EL spectrum of the device based on **SAFpCN** exhibited a slight red shift compared with that of **SAFmCN**, both devices still emitted a deep blue light in the HDTV standard blue colour region (CIE of (0.15, 0.06)).[21] Moreover, these OLEDs also showed narrow EL spectra with a full width at half maximum (FWHM) of 50–56 nm (Fig. 4b), proving a superior colour purity of deep blue colour. The EL spectra are consistent with their PL emissions in the film without emission peaks at lower buffer layers' wavelengths. They show stability by increasing the voltage from 3 to 11 V (Fig. S7, ESI†). This indicates pure EML emissions with effective charge recombination in the EML and excimer emission as well as exciplex emissions from TAPC/EML and EML/TmPyPB interfaces being efficiently suppressed. Accordingly, all devices showed a low turn-on voltage (V_{on}) of 3.2 V (Fig. 4c). The device based on **SAFpCN** achieved excellent EL performance, with a maximum current efficiency (CE_{max}) of 6.54 cd A^{-1}, an EQE_{max} of 4.63%, a slight efficiency roll-off (3.89% at 100 cd m^2; 3.31% at 1000 cd m^2), a maximum luminance (L_{max}) of 3900 cd m^{-2} and a maximum power efficiency (PE_{max}) of 5.63 lm W^{-1} (Fig. 4d). The **SAFmCN**-based device showed somewhat lower EL performance with CE_{max}/EQE_{max} of 3.86 cd A^{-1}/3.18%. To the best of our knowledge, the **SAFpCN**-based device is considered as one of the high EL performance deep blue HLCT-based OLEDs with CIE$y \leq$ 0.05.[8c,21b,22] The high EL efficiency of **SAFpCN**-based devices could be ascribed to the synergetic effects of HLCT character and high and balanced charge mobilities of the emitter, and the optimized device structure. The possible RISC process *via* upper excited states of the HLCT-emitter could somewhat boost up the EQE, whereas a well charge-balanced device could contribute to widen the recombination zone in the EML and result in low driving voltage and long lifetime device.[23] The η_s values of the non-doped devices of **SAFpCN** and **SAFmCN** were calculated to be 51% and 41%,[24] respectively, exceeding the theoretical limit of 25% for traditional fluorescent OLEDs.

Experimental

Materials and methods

All reagents were purchased from Aldrich and TCI companies and used without further purification. Solvents were dried by using standard procedures.

^{1}H-NMR and ^{13}C-NMR spectra were recorded on Bruker Avance-600 MHz spectrometers. High-resolution mass spectra were analyzed using a Bruker microflex MALDI-TOF mass spectrometer. Differential scanning calorimetry (DSC) and thermogravimetric (TGA) analyses were performed using a PerkinElmer DSC-8500 thermal analyzer and a TGA/DSC1 Mettler Toledo with a heating rate of 10 °C min^{-1} under N_2 flow, respectively. UV-visible absorption spectra were recorded on a PerkinElmer UV Lambda 1050 spectrometer. Photoluminescence and lifetime were measured by using a FLS980 Edinburgh fllmer UV Lambda 1050 s. The absolute photoluminescence quantum yield (Φ_{PL}) was determined by using an integrating sphere. Photoelectron spectroscopy (AC-2) was performed on a Riken-Keiki ultraviolet photoelectron spectrometer AC-2 in air. Cyclic voltammetry (CV) measurements were carried out using an Autolab potentiostat PGSTAT 101 equipped with a three-electrode setup (platinum, glassy carbon, and Ag/AgCl). Melting points were measured using a Krüss KSP1N melting point meter and are uncorrected.

The quantum chemical calculations were performed with Gaussian 09 program package using density functional theory (DFT).[25] The HOMO and LUMO distributions of the complexes were calculated with the DFT B3LYP/6-31G(d) function.

OLED devices with non-doped configurations of ITO/MoO_3 (6 nm)/C_{60} (3 nm)/4,4′-cyclohexylidenebis[*N*,*N*-bis(*p*-tolyl)aniline] (TAPC) (20 nm)/**SAFpCN** or **SAFmCN** (40 nm)/1,3,5-tris (3-pyridyl-3-phenyl)benzene (TmPyPB) (55 nm)/LiF (0.5 nm)/Al (150 nm) were fabricated and characterized as followed. The

Table 2 Electroluminescence data of the non-doped EL devices[a]

EML	V_{on} (V)	λ_{EL} (nm)	FWHM (nm)	L_{max} (cd m^{-2})	J_{max} (mA cm^{-2})	EQE_{max}/CE_{max}/PE_{max}[b] (%/cd A^{-1}/lm W^{-1})	CIE (x, y)	η_s (%)
SAFpCN	3.2	432	56	3900	180	4.63/6.54/5.63	0.153, 0.054	51
SAFmCN	3.2	413	50	6420	325	3.18/3.86/2.50	0.160, 0.046	41

[a] ITO/MoO_3 6 nm/C_{60} 3 nm/TAPC 20 nm/EML 40 nm/TmPyPB 55 nm/LiF 0.5 nm/Al 150 nm. [b] External quantum efficiency/luminance efficiency/power efficiency.

cleaned and patterned indium tin oxide (ITO) glass substrate (12 Ω sq^{-1}) was treated by UV ozone for 30 min. MoO_3 (6 nm) and C_{60} (3 nm) as the hole injection layer and TAPC (20 nm) as the hole transport layer were deposited by thermal evaporation at an evaporation rate of 1 Å s^{-1} from low-temperature evaporator sources in a Kurt J. Lasker mini SPECTROS 100 thin film deposition system under a base pressure of 5×10^{-6} bar. A quartz oscillator thickness sensor is used to monitor the film thickness. **SAFpCN** or **SAFmCN** as the EML was then deposited on top with 40 nm thickness. The 55 nm thick TmPyPB as the electron transport layer (ETL), 0.5 nm thick LiF, and 150 nm thick aluminum layers were subsequently deposited through a shadow mask on the top of the EML without breaking the vacuum to form an active diode area of 4 mm^2. Hole and electron only devices with configurations of ITO/NPB 10 nm/**SAFpCN** or **SAFmCN** 80 nm/NPB 10 nm/Al 100 nm and ITO/TmPyPB 10 nm/**SAFpCN** or **SAFmCN** 80 nm/TmPyPB 10 nm/LiF 0.5 nm/Al 100 nm were also fabricated, respectively. Current density–voltage–luminance (*J–V–L*) characteristics were measured simultaneously using a Keithley 2400 source meter and a Hamamatsu Photonics PMA-12 multi-channel analyzer. The absolute external quantum efficiency (EQE) of OLED devices was obtained by using a Hamamatsu Photonics C9920-12 external quantum efficiency measurement system utilizing an integrating sphere. All the measurements were performed under an ambient atmosphere at room temperature.

Synthesis and characterisation

4-(10-Phenyl-10*H*-spiro[acridine-9,9′-fluoren]-2-yl)benzonitrile (SAFpCN). A mixture of 4-cyanophenylboronic acid (0.09 g, 0.61 mmol), **2** (0.20 g, 0.41 mmol), $Pd(PPh_3)_4$ (0.024 g, 0.021 mmol) and 2 M Na_2CO_3 aqueous solution (5 ml) in THF (40 ml) was degassed with N_2 for 5 min and then heated at reflux under an N_2 atmosphere for 24 h. After cooling to room temperature, the mixture was extracted with DCM, washed with water and brine solution, and dried over anhydrous Na_2SO_4 and the organic solvent was removed. The crude product was purified using silica gel column chromatography (40% DCM : hexane) followed by recrystallisation in a mixture of DCM/methanol to obtain a white solid (0.16 g, 68%). M.p. = 276 °C. ^{1}H NMR (600 MHz, $CDCl_3$) δ 7.82 (d, J = 7.6 Hz, 2H), 7.74 (t, J = 7.8 Hz, 2H), 7.61 (t, J = 7.5 Hz, 1H), 7.53 (d, J = 7.2 Hz, 2H), 7.47 (dd, J = 12.1, 8.0 Hz, 4H), 7.40 (td, J = 7.5, 0.7 Hz, 2H), 7.28 (td, J = 7.5, 0.8 Hz, 2H), 7.23 (d, J = 8.4 Hz, 2H), 7.17 (dd, J = 8.7, 2.2 Hz, 1H), 6.95 (ddd, J = 8.5, 7.3, 1.5 Hz, 1H), 6.64 (d, J = 2.2 Hz, 1H), 6.61 (td, J = 7.5, 0.9 Hz, 1H), 6.46 (d, J = 8.7 Hz, 1H), 6.43 (dd, J = 7.8, 1.4 Hz, 1H), 6.39 (d, J = 7.9 Hz, 1H). ^{13}C NMR (151 MHz, $CDCl_3$) δ 156.37, 145.01, 142.08, 141.04, 140.88, 139.37, 132.47, 131.36, 131.11, 131.01, 128.90, 128.64, 127.99, 127.88, 127.52, 126.69, 126.59, 126.15, 125.90, 125.83, 125.04, 121.32, 120.24, 119.27, 115.46, 115.05, 109.69, 57.00. HRSM MALDI-TOF m/z $[M]^+$ calcd for $C_{38}H_{24}N_2$ 508.1939, found 508.4335.

3-(10-Phenyl-10*H*-spiro[acridine-9,9′-fluoren]-2-yl)benzonitrile (SAFmCN). A mixture of 3-cyanophenylboronic acid (0.15 g, 1.01 mmol), **2** (0.33 g, 0.68 mmol), $Pd(PPh_3)_4$ (0.031 g, 0.034 mmol) and 2 M Na_2CO_3 aqueous solution (5 ml) in THF (30 ml) was degassed with N_2 for 5 min and then heated at reflux under a N_2 atmosphere for 24 h. After cooling to room temperature, the mixture was extracted with DCM, washed with water and brine solution, and dried over anhydrous Na_2SO_4 and the organic solvent was removed. The crude product was purified using silica gel column chromatography (40% DCM:hexane) followed by recrystallisation in a mixture of DCM/methanol to obtain a white solid (0.22 g, 64%). M.p. = 280 °C. ^{1}H NMR (600 MHz, $CDCl_3$) δ 7.83 (d, J = 7.6 Hz, 2H), 7.75 (t, J = 7.8 Hz, 2H), 7.61 (t, J = 7.5 Hz, 1H), 7.54 (d, J = 8.2 Hz, 2H), 7.46 (d, J = 7.6 Hz, 2H), 7.44–7.38 (m, 4H), 7.36 (dt, J = 8.1, 1.3 Hz, 1H), 7.32–7.27 (m, 3H), 7.12 (dd, J = 8.7, 2.2 Hz, 1H), 6.94 (ddd, J = 8.8, 7.3, 1.5 Hz 1H), 6.64–6.57 (m, 2H), 6.46 (d, J = 8.7 Hz, 1H), 6.43 (dd, J = 7.8, 1.4 Hz, 1H), 6.39 (d, J = 8.4 Hz, 1H). ^{13}C NMR (151 MHz, $CDCl_3$) δ 156.40, 141.91, 141.84, 141.09, 140.95, 139.37, 131.36, 131.16, 130.87, 130.73, 129.86, 129.80, 129.40, 128.87, 128.64, 128.02, 127.89, 127.49, 126.34, 126.02, 125.89, 125.82, 125.05, 121.22, 120.30, 119.13, 115.49, 115.00, 112.72, 57.01. HRSM MALDI-TOF m/z $[M]^+$ calcd for $C_{38}H_{24}N_2$ 508.1939, found 508.3551.

Conclusions

In summary, we have developed a simple design and structure of D–A-based deep blue emitters bearing spiro-acridine as donors and cyanophenyl as acceptors. The materials exhibit HLCT characters with strong ultra-deep blue emissions in both solution and film states with emission peaks at 410–433 nm. The non-doped OLED fabricated with **SAFpCN** emits deep blue color in the HDTV standard blue region with a narrow full-width at half maximum of 56 nm, CIE of (0.153, 0.054), a brightness of 3900 cd m^{-2}, a CE_{max} of 6.54 cd A^{-1}, an EQE_{max} of 4.63% and a singlet exciton utilization efficiency of 51%. These results offer a straightforward approach to design HLCT-based deep blue fluorescent molecules suitable for fabricating efficient and stable non-doped deep blue EL devices.

Author contributions

T. S.: investigation, data curation and writing – original draft preparation. S. P., C. K., C. C., P. W., S. N., and P. C.: investigation and data curation. V. P.: supervision, funding acquisition and writing – reviewing and editing.

Conflicts of interest

There are no conflicts to declare.

Acknowledgements

We acknowledged the financial support from the Thailand Research Fund (RTA6080005) and NANOTEC, NSTDA, Ministry of Science and Technology, Thailand, through its program of Research Network NANOTEC. Many thanks also go to Vidyasirimedhi Institute of Science and Technology for supporting both Postdoctoral Fellowship (to T. S.) and equipment.

Notes and references

1 (*a*) J. H. Lee, C. H. Chen, P. H. Lee, H. Y. Lin, M. K. Leung, T. L. Chiu and C. F. Lin, *J. Mater. Chem. C*, 2019, **7**, 5874; (*b*) Y. Im, S. Y. Byun, J. H. Kim, D. R. Lee, C. S. Oh, K. S. Yook and J. Y. Lee, *Adv. Funct. Mater.*, 2017, **27**, 1603007.

2 (*a*) C. Fu, S. Luo, Z. Li, X. Ai, Z. Pang, C. Li, K. Chen, L. Zhou, F. Li, Y. Huang and Z. Lu, *Chem. Commun.*, 2019, **55**, 6317; (*b*) A. K. Pal, S. Krotkus, M. Fontani, C. F. R. Mackenzie, D. B. Cordes, A. M. Z. Slawin, I. D. W. Samuel and E. Zysman-Colman, *Adv. Mater.*, 2018, **30**, 1704961.

3 (*a*) M. Godumala, S. Choi, M. J. Cho and D. H. Choi, *J. Mater. Chem. C*, 2019, **7**, 2172; (*b*) D. Wang, C. Cheng, T. Tsuboi and Q. Zhang, *CCS Chem.*, 2020, **2**, 1278.

4 (*a*) Z. Xu, B. Z. Tang, Y. Wang and D. Ma, *J. Mater. Chem. C*, 2020, **8**, 2614; (*b*) C. Poriel and J. Rault-Berthelot, *Adv. Funct. Mater.*, 2020, **30**, 1910040; (*c*) S. Wang, M. Qiao, Z. Ye, D. Dou, M. Chen, Y. Peng, Y. Shi, X. Yang, L. Cui, J. Li, C. Li, B. Wei and W.-Y. Wong, *iScience*, 2018, **9**, 532.

5 X. Yang, X. Xu and G. Zhou, *J. Mater. Chem. C*, 2015, **3**, 913.

6 (*a*) K. Klimes, Z. Q. Zhu and J. Li, *Adv. Funct. Mater.*, 2019, **29**, 1903068; (*b*) X. C. Hang, T. Fleetham, E. Turner, J. Brooks and J. Li, *Angew. Chem., Int. Ed.*, 2013, **52**, 6753.

7 K. Matsuo and T. Yasuda, *Chem. Sci.*, 2019, **10**, 10687.

8 (*a*) W. Li, Y. Pan, L. Yao, H. Liu, S. Zhang, C. Wang, F. Shen, P. Lu, B. Yang and Y. Ma, *Adv. Opt. Mater.*, 2014, **2**, 892; (*b*) X. Lv, M. Sun, L. Xu, R. Wang, H. Zhou, Y. Pan, S. Zhang, Q. Sun, S. Xue and W. Yang, *Chem. Sci.*, 2020, **11**, 5058; (*c*) W. C. Chen, Y. Yuan, S. F. Ni, Q. X. Tong, F. L. Wong and C. S. Lee, *Chem. Sci.*, 2017, **8**, 3599; (*d*) H. Zhang, B. Zhang, Y. Zhang, Z. Xu, H. Wu, P.-A. Yin, Z. Wang, Z. Zhao, D. Ma and B. Z. Tang, *Adv. Funct. Mater.*, 2020, **30**, 2002323; (*e*) H. Zhang, J. Zeng, W. Luo, H. Wu, C. Zeng, K. Zhang, W. Feng, Z. Wang, Z. Zhao and B. Z. Tang, *J. Mater. Chem. C*, 2019, **7**, 6359; (*f*) C. Zhou, S. Xiao, M. Wang, W. Jiang, H. Liu, S. Zhang and B. Yang, *Front. Chem.*, 2019, **7**, 141; (*g*) C. Wang, X.-L. Li, Y. Gao, L. Wang, S. Zhang, L. Zhao, P. Lu, B. Yang, S.-J. Su and Y. Ma, *Adv. Opt. Mater.*, 2017, **5**, 1700441; (*h*) W. Xie, B. Li, X. Cai, M. Li, Z. Qiao, X. Tang, K. Liu, C. Gu, Y. Ma and S.-J. Su, *Front. Chem.*, 2019, **7**, 276.

9 (*a*) M. Kim, J. M. Choi and J. Y. Lee, *Chem. Commun.*, 2016, **52**, 10032; (*b*) C. Y. Chan, L. S. Cui, J. U. Kim, H. Nakanotani and C. Adachi, *Adv. Funct. Mater.*, 2018, **28**, 1706023.

10 W. Z. Yuan, X. Bin, G. Chen, Z. He, J. Liu, H. Ma, Q. Peng, B. Wei, Y. Gong, Y. Lu, G. He and Y. Zhang, *Adv. Opt. Mater.*, 2017, **5**, 1700466.

11 (*a*) J. Tagare and S. Vaidyanathan, *J. Mater. Chem. C*, 2018, **6**, 10138; (*b*) B. Liu, Z. W. Yu, D. He, Z. L. Zhu, J. Zheng, Y. D. Yu, W. F. Xie, Q. X. Tong and C. S. Lee, *J. Mater. Chem. C*, 2017, **5**, 5402.

12 (*a*) Y. Liu, H. Liu, Q. Bai, C. Du, A. Shang, D. Jiang, X. Tang and P. Lu, *ACS Appl. Mater. Interfaces*, 2020, **12**, 16715; (*b*) X. Chen, Z. Yang, W. Li, Z. Mao, J. Zhao, Y. Zhang, Y. C. Wu, S. Jiao, Y. Liu and Z. Chi, *ACS Appl. Mater. Interfaces*, 2019, **11**, 39026; (*c*) H. Usta, D. Alimli, R. Ozdemir, S. Dabak, Y. Zorlu, F. Alkan, E. Tekin and A. Can, *ACS Appl. Mater. Interfaces*, 2019, **11**, 44474; (*d*) V. Thanikachalam, P. Jeeva and J. Jayabharathi, *RSC Adv.*, 2017, **7**, 13604; (*e*) Z. Li, N. Xie, Y. Xu, C. Li, X. Mu and Y. Wang, *Org. Mater.*, 2020, **2**, 11.

13 X. Qiu, Y. Xu, C. Wang, M. Hanif, J. Zhou, C. Zeng, Y. Li, Q. Jiang, R. Zhao, D. Hu and Y. Ma, *J. Mater. Chem. C*, 2019, **7**, 5461.

14 W. Sun, N. Zhou, Y. Xiao, S. Wang and X. Li, *Dyes Pigm.*, 2018, **154**, 30.

15 T. Liu, H. Sun, C. Fan, D. Ma, C. Zhong and C. Yang, *Org. Electron.*, 2014, **15**, 3568.

16 F. Liu, Y. Tan, H. Liu, X. Tang, L. Gao, C. Du, J. Min, H. Jin and P. Lu, *J. Mater. Chem. C*, 2020, **8**, 6883.

17 R. Chen, Y. Tang, Y. Wan, T. Chen, C. Zheng, Y. Qi, Y. Cheng and W. Huang, *Sci. Rep.*, 2017, **7**, 6225.

18 S. Zhang, L. Yao, Q. Peng, W. Li, Y. Pan, R. Xiao, Y. Gao, C. Gu, Z. Wang, P. Lu, F. Li, S. Su, B. Yang and Y. Ma, *Adv. Funct. Mater.*, 2015, **25**, 1755.

19 Y. Li, R. G. Clevenger, L. Jin, K. V. Kilway and Z. Peng, *J. Mater. Chem. C*, 2014, **2**, 7180.

20 S. Wu, S. Li, Q. Sun, C. Huang and M. K. Fung, *Sci. Rep.*, 2016, **6**, 25821.

21 (*a*) T. Shan, Y. Liu, X. Tang, Q. Bai, Y. Gao, Z. Gao, J. Li, J. Deng, B. Yang, P. Lu and Y. Ma, *ACS Appl. Mater. Interfaces*, 2016, **8**, 28771; (*b*) G. Li, J. Zhao, D. Zhang, J. Zhu, Z. Shi, S. Tao, F. Lu and Q. Tong, *New J. Chem.*, 2017, **41**, 5191.

22 (*a*) W. C. Chen, Y. Yuan, Y. Xiong, A. L. Rogach, Q. X. Tong and C. S. Lee, *ACS Appl. Mater. Interfaces*, 2017, **9**, 26268; (*b*) X. Qiu, S. Ying, C. Wang, M. Hanif, Y. Xu, Y. Li, R. Zhao, D. Hu, D. Ma and Y. Ma, *J. Mater. Chem. C*, 2019, **7**, 592.

23 S. W. Culligan, A. C. A. Chen, J. U. Wallace, K. P. Klubek, C. W. Tang and S. H. Chen, *Adv. Funct. Mater.*, 2006, **16**, 1481.

24 J. Jayabharathi, G. Goperundevi, V. Thanikachalam and S. Panimozhi, *ACS Omega*, 2019, **4**, 15030.

25 M. J. Frisch, G. W. Trucks, H. B. Schlegel, G. E. Scuseria, M. A. Robb, J. R. Cheeseman, G. Scalmani, V. Barone, B. Mennucci, G. A. Petersson, H. Nakatsuji, M. Caricato, X. Li, H. P. Hratchian, A. F. Izmaylov, J. Bloino, G. Zheng, J. L. Sonnenberg, M. Hada, M. Ehara, K. Toyota, R. Fukuda, J. Hasegawa, M. Ishida, T. Nakajima, Y. Honda, O. Kitao, H. Nakai, T. Vreven, J. A. Montgomery, Jr., J. E. Peralta, F. Ogliaro, M. Bearpark, J. J. Heyd, E. Brothers, K. N. Kudin, V. N. Staroverov, R. Kobayashi, J. Normand, K. Raghavachari, A. Rendell, J. C. Burant, S. S. Iyengar, J. Tomasi, M. Cossi, N. Rega, J. M. Millam, M. Klene, J. E. Knox, J. B. Cross, V. Bakken, C. Adamo, J. Jaramillo, R. Gomperts, R. E. Stratmann, O. Yazyev, A. J. Austin, R. Cammi, C. Pomelli, J. W. Ochterski, R. L. Martin, K. Morokuma, V. G. Zakrzewski, G. A. Voth, P. Salvador, J. J. Dannenberg, S. Dapprich, A. D. Daniels, Ö. Farkas, J. B. Foresman, J. V. Ortiz, J. Cioslowski and D. J. Fox, *Gaussian 09*, Gaussian, Inc., Wallingford CT, 2009.